Studies of permittivity and permeability of dielectric matrix with cuboid metallic inclusions in different orientations

JOURNAL OF ADVANCED DIELECTRICS
Vol. 4, No. 4 (2014) 1450032 (8 pages)

DOI: 10.1142/S2010135X14500325

World Scientific
www.worldscientific.com

Studies of permittivity and permeability of dielectric matrix with cuboid metallic inclusions in different orientations

W. M. Wu[†,§], C. C. Njoku[‡], W. G. Whittow[‡], A. M. Zagoskin[†], F. V. Kusmartsev[†] and J. C. Vardaxoglou[‡]
[†]*Department of Physics, Loughborough University*
Loughborough LE11 3TU, United Kingdom
and
[‡]*School of Electronic, Electrical and Systems Engineering*
Loughborough University, Loughborough LE11 3TU
United Kingdom
[§]phwmw2@lboro.ac.uk

Received 22 September 2014; Accepted 3 November 2014; Published 28 November 2014

In this paper, we investigate the possibility of using the heterogeneous materials, with cuboid metallic inclusions inside a dielectric substrate (host) to control the effective permittivity. We find that in the gigahertz range, such a material demonstrates a significantly larger permittivity compared to the pure dielectric substrate. Three principal orientations of microscale cuboid inclusions have been taken into account in this study. The highest permittivity is observed when the orientation provides the largest polarization (electric dipole moment). The detrimental side effect of the metallic inclusion, which leads to the decrease of the effective magnetic permeability, can be suppressed by the proper choice of shape and orientation of the inclusions. This choice can in fact reduce the induced current and hence maximize the permeability. The dissipative losses are shown to be negligible in the relevant range of frequencies and cuboid dimensions.

Keywords: Permittivity; cuboid; orientation; antenna; inclusions.

1. Introduction

In this paper, we study the effective permittivity ϵ_{eff} and permeability μ_{eff}, of a dielectric substrate (host) with microscale metallic inclusions. Our aim is to increase the effective permittivity (dielectric constant) for dielectric materials. The wavelength in high ϵ_{eff} materials is reduced and therefore, the electromagnetic devices (e.g., antennas) can be miniaturized.[1,2] Recent studies find that small metallic inclusions in a dielectric host can offer a high effective permittivity.[3–5] In general, the permittivity of a host is selected to be as small as possible in the design. The host with low permittivity could reduce the wave reflections at the interface between the air and substrate,[6] and this could improve the efficiency of the devices.[1,6]

The dielectric substrate can be sub-divided into many cubic unit cells (basic building blocks) (Fig. 1). Each inclusion is situated at the center of each unit cell (Fig. 2). It is assumed that all inclusions are parallel to each other, and are not randomly located.[7–10]

Typically, the volume ratio of an inclusion to a unit cell (volume fraction) is one of the key factors, which determines the effective permittivity of the mixture.[3–5,8–10] The range of frequency is also important to the value of effective permittivity,[3–5] and we focus on the 10 GigaHertz range in our case.[3–5,10]

The inclusion shape also plays an important role to the values of effective permittivity and permeability. Several studies on isotropic geometries can be found in literature.[3–5,10] For example, existing theories (i.e., the extended Maxwell–Garnett formula[10]) describe the metallic spherical inclusions for dielectric mixtures very well, and is approximated by

$$\epsilon_{\text{eff}} = \epsilon_{\text{H}} + 3\epsilon_{\text{H}} \frac{V_r}{1 - V_r}, \tag{1}$$

where ϵ_{H} is the permittivity of the host substrate, and V_r is the volume fraction.[11–15] Needless to say, it is not a simple task for calculating the values of effective permittivity with anisotropic inclusions,[16–24] and the effective permittivity varies from different orientations of inclusions.

The cuboid (square shape with a finite thickness) metallic inclusions have been analyzed in our studies. However, the values of relative ϵ_{eff} and μ_{eff} have been controlled, by choosing suitable orientations and dimensions of the inclusions. We will also discuss how the polarization and eddy current are associated with ϵ_{eff} and μ_{eff}, respectively, in an

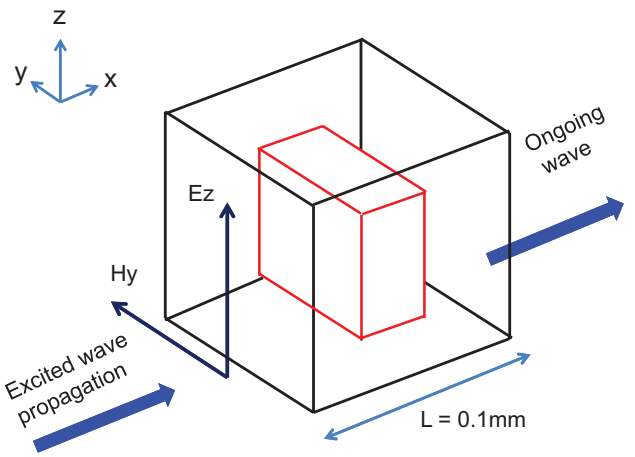

Fig. 1. A thin square cuboid inclusion in a cubic unit cell. This is the basic building block of the cuboid inclusion. The direction of propagation is along the x-axis, while the electric and magnetic fields are in z-axis and y-axis, respectively. The cuboid is allocated at the center of the unit cell.

applied electromagnetic field, with respect to the three principal orientations using classical theory.[25–27]

2. Theory and Methodology

2.1. *Frequency range*

In this numerical study, the domain host is made up of many cubic unit cells, and the sides of the cubic cell are 10^{-4}m. The incident wave is taken to be a plane wave, and it propagates through the substrate along the x-axis (where the electric **E** field is parallel to the z-axis, and the magnetic **H** field to the y-axis). The wavelength λ, must be at least, 10 times larger than the side of the cubic unit cell L, $\lambda > 10L$.[26] The large λ minimizes the reflection and scattering from inclusions.[25,26] Given the size of λ, the frequency limit is $\sim 10^{11}$ Hz, and this work is confined to the range 1–50 GHz. The skin depth of silver is approximated 10^{-6} m at 10 GHz,[27] and this scale is much smaller than the size of the unit cell of the substrate (10^{-4} m). Therefore, the loss tangents (complex parts) of the ϵ_{eff} and μ_{eff} of the overall substrate, are theoretically small.[28,29] Generally speaking, the size of the inclusions, unit cell and frequency range can be rescaled according to the above constraints.

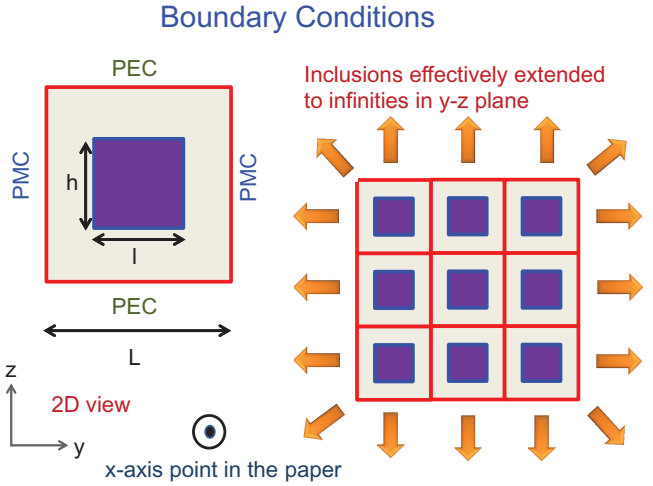

Fig. 2. The 2D view (y–z plane) of the inclusion. The boundary conditions: perfect electric conductors (PECs) and perfect magnetic conductor (PMC) are assigned to the surfaces of substrate. These boundaries are effectively equivalent to an infinite number of unit cells on the y–z plane. There are M layers of until cell along the x-axis.

2.2. *Inclusion material and volume fraction*

The choice of material is crucial to the values of relative ϵ_{eff} and μ_{eff}. In this study, the host substrate is chosen to be a pure dielectric (e.g., polymers), while the metallic inclusions are made of silver (Ag). The conductivity, relative permittivity and permeability, of the host substrate are $(\sigma_{\text{H}}, \epsilon_{\text{H}}, \mu_{\text{H}}) = (0, 1.5, 1)$; while the conductivity and relative permittivity for silver inclusions are $(\sigma_{\text{I}}, \mu_{\text{I}}) = (6.1 \times 10^7\, S/m, 1)$. The cuboid (anisotropic shape) inclusions, considered in this paper, have length l (parallel to y-axis), height h (parallel to z-axis) and thickness w (parallel to x-axis). We further set the dimension of length l and height h are equal ($h = l$) for simplicity, and

$$l, h, w < L. \tag{2}$$

The shape of this cuboid looks like a square layer, with a finite thickness w (Figs. 1 and 2).

The volume fraction V_r is a volume ratio of the inclusion to the unit cell, and is defined as

$$V_r = \frac{wlh}{L^3}. \tag{3}$$

As mentioned before, the values of relative ϵ_{eff} and μ_{eff} are usually determined mainly by the volume fraction V_r. The geometry and orientation of inclusion also play an important role for these values, and we will analyze this in later sections.

2.3. *Boundary conditions*

The boundary conditions of the top and bottom surfaces of the substrate (perpendicular to z-axis), are those PECs; while the left and right surfaces (perpendicular to y-axis) are set to be PMCs.[3–5,8] These conditions effectively provide an infinite array of periodic unit cells on the y–z plane (H–E plane) (Fig. 2). Finally, the front and back boundaries (perpendicular to x-axis) of the substrate are set to be an excited

wave, and ongoing wave, respectively (Fig. 1). These conditions allow the scattering wave to travel freely throughout the substrate.[3–5] There are M unit cells along the propagated direction x. Practically, it is sufficient to allocate about five cells ($M = 5$), so that ϵ_{eff} and μ_{eff} converge — for which the scattering fields between inclusions are reasonably averaged out. Therefore, five cell layers along the direction x is used in the model for simplicity.

2.4. *Formula of model*

The differential Drude–Maxwell model,[25,27,30] with electric field **E**, has been employed in the numerical simulation (Finite Element Methods in Comsol), and is given by

$$\nabla \times \nabla \times \mathbf{E} - \mu_r k_0^2 \left(\epsilon_r - \frac{i\sigma}{\omega \epsilon_0}\right)\mathbf{E} = 0, \tag{4}$$

where $k_0 = 2/\lambda_0$ is the wave vector number, and λ_0 is a wavelength in a free space. ϵ_r and μ_r are the relative permittivity and permeability of the corresponding material itself, whilst ϵ_0 is a free space permittivity. $\omega = 2\pi f$ is the angular frequency, and σ is the conductivity which is assumed to be a constant in the Drude–Maxwell model. The electric field **E** in (Eq. (4)) can be alternatively replaced by the magnetic field **H**, and they are equivalent to each other in theory.

Polarization **P** and magnetization **M** are the key physical quantities to understand the ϵ_{eff} and μ_{eff} inside the system. In macroscopic view, the polarization **P** measures how a dielectric responds to the **E** field[17–19,25,31–33] (Fig. 3). Its relationship can be linked by the electric susceptibility χ_e

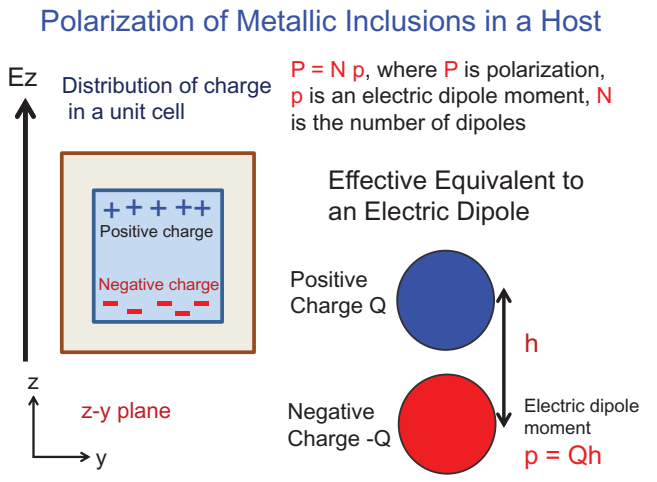

Fig. 3. The figure shows a host substrate with metallic inclusions, in an electric field. Each unit cell with an inclusion can be regarded as a small electric dipole. Summing all the N electric dipoles (microscopic) can be effectively equivalent to the polarization (macroscopic view), $\mathbf{P} = N\mathbf{p}$. Actually, polarization **P** measures the response of a material to the electric field **E**, and it is linked to the effective permittivity.

(in tensor form),

$$\mathbf{P} = \epsilon_0 \chi_e \mathbf{E}. \tag{5}$$

The total displacement field **D** is equal to the sum of the **E** field and polarization **P** (local field); that is, $\mathbf{D} = \epsilon_0 \epsilon_r \mathbf{E} = \epsilon_0 \mathbf{E} + \mathbf{P}$, where $\epsilon_r = \chi_e + 1$.[17–19,25,32,33] It is also assumed that **P** oscillates in phase to an applied **E** field. **P** can be also associated with the electric dipole moment **p** in the microscopic view, $\mathbf{P} = N\mathbf{p}$, where N is the number of dipole per unit volume.[25] Actually, each dielectric unit cell with a metallic inclusion can be effectively regarded as the electric dipole, and the dipole moment is

$$\mathbf{p} = Q\mathbf{h}, \tag{6}$$

where **h** is the height of an inclusion with direction along the z-axis.

Similar to the polarization **P**, magnetization **M** measures how a material responds to an applied magnetic field **H**, and is represented by,

$$\mathbf{M} = \chi_m \mathbf{H}, \tag{7}$$

where χ_m is the magnetic susceptibility. The total magnetic field **B** in the system is sum of **H** and **M**, so that, $\mathbf{B} = \mu_0(\mathbf{H} + \mathbf{M}) = \mu_0 \mu_r \mathbf{H}$, where $\mu_r = \chi_m + 1$.[17–19,25] Details of the magnetization (i.e., paramagnetic, ferromagnetic) can be reviewed from the literature.[34–38]

2.5. *Scattering parameters*

In this simulation scheme, an inverse scattering procedure has been applied to evaluate the permittivity and permeability of the heterogeneous substrate.[5,39–41] This inverse process is in fact a numerical method — which estimates the ϵ_{eff} and μ_{eff} from scattering parameters (S-parameters). It is important to note that this method relies on certain assumptions. The S-parameters, $S_{11} = E_R/E_I$ (reflection) and $S_{21} = E_T/E_I$ (transmission) should be less than one, $|S_{11}| < 1$ and $|S_{21}| < 1$, where E_I, E_R and E_T are the incident, reflected and transmitted electric fields correspondingly.[25,39–41] The impedance **Z** is assumed to be dependent on the effective permittivity and permeability only,[5,39–41] and is given by

$$\mathbf{Z} = \sqrt{\frac{\mu_{\text{eff}}}{\epsilon_{\text{eff}}}}. \tag{8}$$

The phase θ of the EM wave must be continuous, and it provides the information of the length of propagation. The propagation constant κ can be extracted from the phase θ, and is also related to

$$\kappa = \kappa_0 \sqrt{\mu_{\text{eff}} \epsilon_{\text{eff}}}, \tag{9}$$

where κ_0 is the propagation constant in the free space. Once **Z** and κ are estimated, one can determine μ_{eff} and ϵ_{eff}. The detailed procedure is described in Refs. 4, 5 and 39–41.

3. Simulation Results and Discussions

3.1. *Metallic cubic inclusions*

Recalling our major objective is to increase the value of relative ϵ_{eff} of the whole substrate, by inserting the silver (Ag) inclusions. The relative permittivity of the host is assumed to $\epsilon_H = 1.5$ and lossless for simplicity. To validate the model, silver cubic inclusions are initially investigated. This also allows comparison with cuboid inclusions. As mentioned in Sec. 2, the sides (length) of the unit cell are $L = 10^{-4}$ m, and the EM wave frequency is in the range of 1–50 GHz. Three sizes of silver cubic inclusions (Fig. 4) are selected with the sides 0.6×10^{-4}, 0.8×10^{-4} and 0.9×10^{-4} m. The volume fractions are 0.216, 0.512 and 0.729, respectively. The relative ϵ_{eff} and μ_{eff} of these configurations are shown in Fig. 4. It is obvious that the ϵ_{eff} rises, as the volume fraction of cubic inclusion increases. When the volume fraction is 0.729, the average value of ϵ_{eff} is $14.634 + 0.0005i$ (with a small complex component). The effective dielectric constant of the whole substrate is more than nine times of the dielectric host itself ($\epsilon_H = 1.5$). For the volume fractions 0.216 and 0.512, the average of ϵ_{eff} (in the frequency range of 1–50 GHz) are 3.079 and $6.949 - 0.0001i$, respectively. We also discover that the values of ϵ_{eff} are almost flat with respect to the frequency. Therefore, it is reasonable to fix this at the frequency $f = 10$ GHz, and to consider the change of ϵ_{eff} to the volume fraction V_r. Figure 5 shows that ϵ_{eff} increases versus the volume fraction V_r. The blue solid line stands for the cubic inclusions calculated by the Drude–Maxwell model. In the simulations, ϵ_{eff} can even reach to $29.871 + 0.0003i$, with a volume fraction 0.857. We also apply the approximated Maxwell–Garnett formula (by Lewin)[10] for the spherical metallic inclusions, and it is plotted by red '*' in Fig. 5. It is found that the metallic cubic and spherical inclusions provide the similar values of ϵ_{eff} and μ_{eff}, for the same volume fractions. In fact, metallic inclusions can offer a higher permittivity originating from the term of $j\sigma/(\omega\epsilon_0)$ in the Drude–Maxwell model.[25] With an applied **E** field, positive or negative charges (Q or $-Q$) accumulate near the upper or bottom edge of an inclusion in the unit cell, and these charges oscillate along with the field. Since the host is made of dielectric material, there is no actual current **J** flow from one cell to another. With silver inclusions (plenty of free charges), the dipole moment $\mathbf{p} = Q\mathbf{h}$ has been enhanced for a whole substrate, as well as the polarization **P** (and hence the effective permittivity).[17–19,25]

On the other hand, the effective permeability drops as the volume fraction V_r increases[10] (Figs. 4 and 5). According to Fig. 4, the average relative μ_{eff} are $0.687 + 0.0042i$, $0.376 + 0.0044i$ and $0.195 + 0.0053i$, for the three volume fractions 0.216, 0.512 and 0.729, respectively. Figure 5 shows that μ_{eff} even drops to $0.102 + 0.0126i$ at $V_r = 0.857$. When the size of a cubic inclusion increases, the surface area becomes bigger at the same time. This leads to an increase of the rate of change of magnetic flux — which is directly proportional to the surface area. According to Lenz's law, the magnetization **M** is generated and opposes to the applied magnetic field **H**. As a result, the μ_{eff} drops (Sec. 2.4).[23–25,27] It is to remind that our task is to keep the values of permeability and permittivity as close as possible, in order to maximize the efficiency of the system.[1]

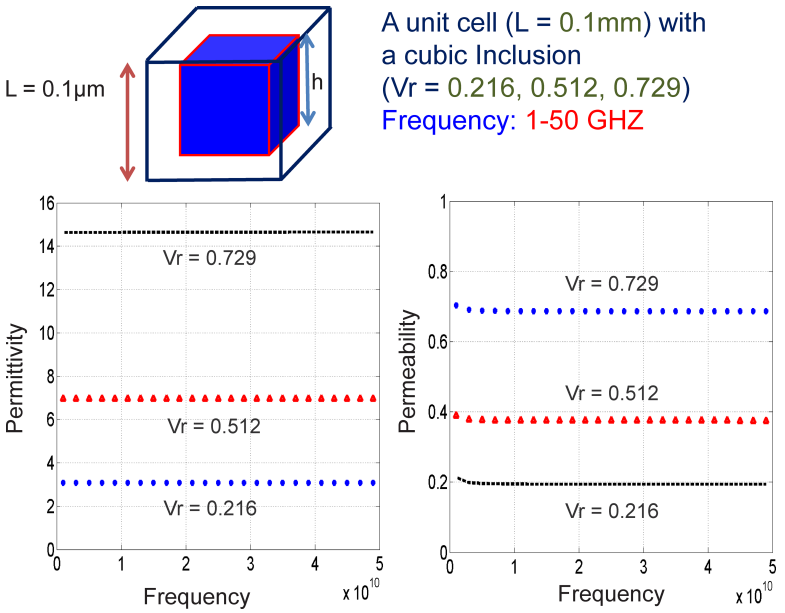

Fig. 4. The figure shows the relative ϵ_{eff} and μ_{eff} of silver cubic inclusion in the frequency (1–50 GHz). The ϵ_{eff} and μ_{eff} remains flat with respect to the frequency. There are three volume fractions 0.216, 0.512 and 0.729. The average ϵ_{eff} are 3.079, $6.949 - 0.0001i$ and $14.634 + 0.0005i$; and the average μ_{eff} are $0.687 + 0.0042i$, $0.376 + 0.0044i$ and $0.195 + 0.0053i$, respectively.

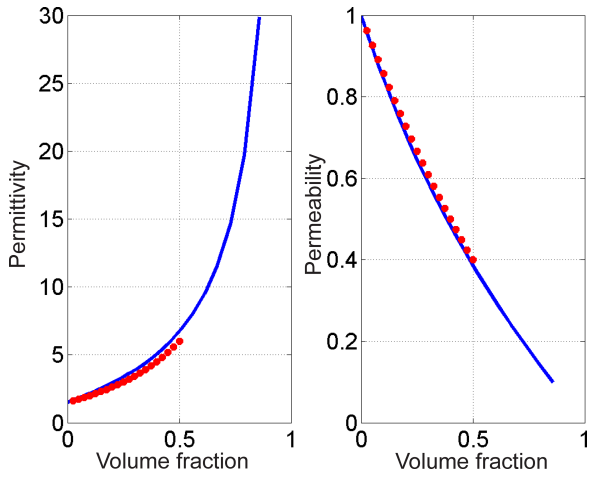

Fig. 5. (Color online) The figure shows the real part of relative ϵ_{eff} and μ_{eff} versus the volume fraction V_r. The blue solid line stands for the cubic inclusions calculated by the Drude–Maxwell model. The red '*' represents the results for spherical inclusions estimated by the approximated Maxwell–Garnett equation (by Lewin). In general, the permittivity rises exponentially when the volume fraction V_r increases. Conversely, the permeability decreases as the volume fraction V_r increases.

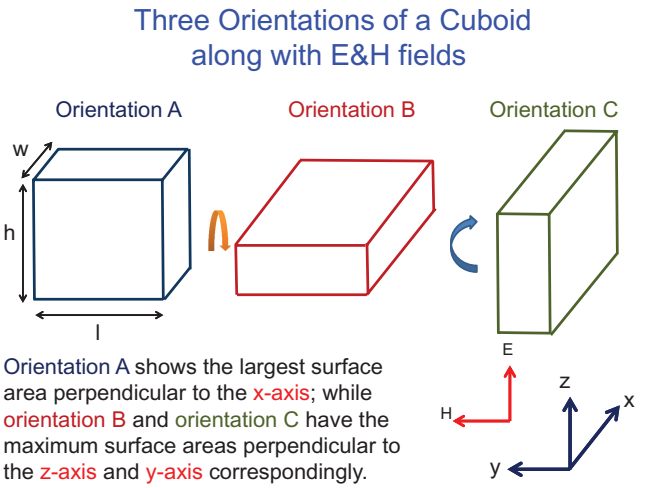

Fig. 6. The figure shows the three principal orientations of the cuboid, the height h, length l and width w, where $l = h > w$. The electric and magnetic fields are along the z-axis and y-axis, respectively, and the direction of propagation is parallel to the x-axis.

Therefore, our second objective is to optimize the relative ϵ_{eff} and μ_{eff}, by adjusting the dimensions and orientation of the cuboids. As we discussed in Sec. 2.2, the thin square cuboid is chosen in our simulation. This is because the thin layer can significantly reduce the induced eddy current **J**, in some orientations. Moreover, the square layer surface helps increase the (electric dipole moment) polarization.[23,24] For silver, the relative permeability is approximately one (i.e., $\mu_{\text{eff}} \sim 1$). Our aim is to maintain the relative μ_{eff} close to one, in the high frequency electromagnetic field.

3.2. *Three orientations of cuboid inclusions*

The electric and magnetic fields in heterogeneous material are not uniformly distributed throughout the substrate. Therefore, ϵ_{eff} and μ_{eff} are represented by 3×3 tensor matrices.[17–19] For simplicity, we only evaluate the values of relative ϵ_{eff} and μ_{eff}, for three principal orientations, assuming the direction of fields is fixed (as shown in Fig. 6). The figure shows a single cuboid inclusion, with three specific orientations — for which the largest surface areas are perpendicular to the x-axis, z-axis and y-axis, respectively. As the unit cell is periodic, all the inclusions in the substrate are parallel to each other, and allocated in the same orientation.

Figure 6 shows the cuboid inclusion in three orientations A, B and C. The dimensions of the inclusion are, 0.9×10^{-4}, 0.9×10^{-4} and 0.2×10^{-4} m, and thus the volume fraction is fixed at $V_r = 0.162$ (less than 20%). It is important to avoid inclusions touching each other, and prevent current flow between inclusions. We summarize the ϵ_{eff} and μ_{eff} of metallic cubic, and cuboid inclusions in orientations A, B and C, in Table 1. The relative permittivity of the orientations A and C are $\epsilon_{\text{A,eff}} = 6.254 + 0.0002i$ and $\epsilon_{\text{C,eff}} = 6.277 - 0.0003i$, respectively; while it is only $\epsilon_{\text{B,eff}} = 1.873$ in orientation B (Figs. 7–9). Compared to silver cubic inclusions, with the same volume fraction (length $= 0.545 \times 10^{-4}$ m), the value of relative ϵ_{eff} is 2.637 (Figs. 4 and 5). It is obvious that the orientations A and C offer higher values of ϵ_{eff}, than cubic and square cuboid inclusions in orientation B. Actually, the heights in the z-axis of inclusions in orientations A and C are 0.9×10^{-4} m, respectively; while the h is only 0.2×10^{-4} m in orientation B (Fig. 6). As a result, the electric dipole moment ($\mathbf{p} = Q\mathbf{h}$) in the orientations A and C are greater than in B, as shown in the simulations (where Q represents the induced charges near the edges of the inclusion). As mentioned previously (Sec. 2.4), the polarization **P** is the average value of all electric dipoles. The higher value of **P** would lead to the higher value permittivity ϵ_{eff} in the system, and thus $\epsilon_{\text{A,eff}} \approx \epsilon_{\text{C,eff}} > \epsilon_{\text{B,eff}}$.

The values of relative permeability are $\mu_{\text{A,eff}} = 0.822 + 0.0029i$, $\mu_{\text{B,eff}} = 0.824 + 0.0029i$ and $\mu_{\text{C,eff}} = 0.417 + 0.0095i$, in orientations A, B and C, respectively (Figs. 7–9). Consider the case of cubic inclusions, with the same volume fraction (0.162), the relative μ_{eff} is $0.757 + 0.004i$ (Fig. 5). In all cases, the relative μ_{eff} is smaller than unity. The simulation results show that μ_{eff} in orientations A and B offer the highest

Table 1. Permittivity and permeability of metallic cubic, and cuboid inclusions in orientations A, B and C.

$V_r = 0.162$	Permittivity (ϵ_{eff})	Permeability (μ_{eff})
Cube	2.637	$0.757 + 0.004i$
Orientation A	$6.254 + 0.0002i$	$0.822 + 0.0029i$
Orientation B	1.873	$0.824 + 0.0029i$
Orientation C	$6.277 - 0.0003i$	$0.417 + 0.0095i$

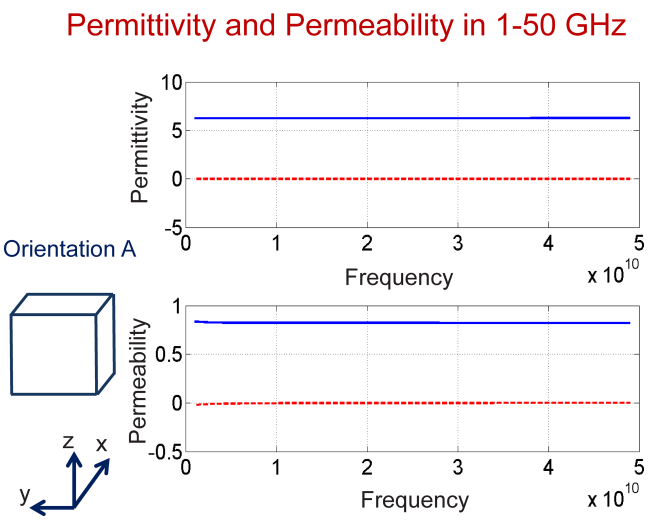

Fig. 7. (Color online) The relative permittivity $\epsilon_{A,eff}$ and permeability $\mu_{A,eff}$ in orientation A. The volume fraction is 0.162. The upper figure refers to the permittivity versus frequency (1–50 GHz); while the lower figure refers to the permeability. The blue solid line and the red dashed line represent the real and imaginary parts, respectively. The average permittivity and permeability are $\epsilon_{A,eff} = 6.254 + 0.0002i$ and $\mu_{A,eff} = 0.822 + 0.0029i$, respectively.

value. The applied magnetic field **H** is pointing toward a lateral surface LS of an inclusion along the y-direction (Fig. 10). The lateral surface (LS $= h \times w$) of an inclusion is shown in Fig. 10. Generally, the induced eddy current (change of total magnetic flux $\Delta\phi$) is proportional to the lateral surface area. Note that μ_{eff} is inversely proportional to the eddy current.[25,27] So that the smaller the induced current, the larger the μ_{eff}. The lateral surface area for orientations A and B is the same, $0.18 \times 10^{-8}\text{m}^2$, so that they render a similar permeability $\mu_{A,eff} \approx \mu_{B,eff}$. Nevertheless, the lateral

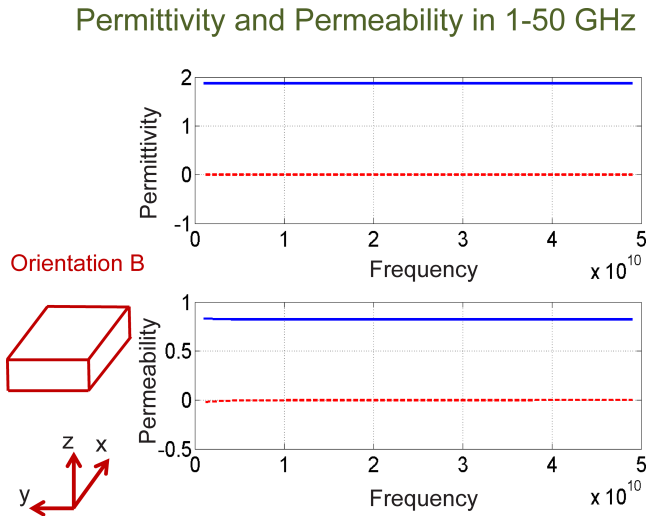

Fig. 8. The relative permittivity $\epsilon_{B,eff}$ and permeability $\mu_{B,eff}$ in orientation B. The average permittivity and permeability are $\epsilon_{B,eff} = 1.873$ and $\mu_{B,eff} = 0.824 + 0.0029i$, respectively.

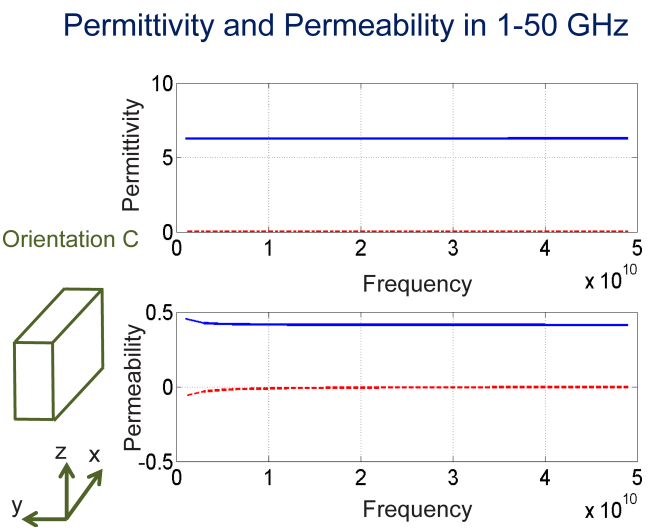

Fig. 9. The figure shows the relative permittivity $\epsilon_{C,eff}$ and permeability $\mu_{C,eff}$ in orientation C. The average permittivity and permeability are $\epsilon_{C,eff} = 6.277 - 0.0003i$ and $\mu_{C,eff} = 0.417 + 0.0095i$, respectively.

surface area LS in orientation C is $0.81 \times 10^{-8}\text{m}^2$, and it provides a large opposing magnetic flux. As a result, the total magnetic field **B** has been reduced, and it causes further drop of the permeability $\mu_{C,eff}$. The complex part of $\mu_{C,eff}$ is $0.0095i$, and it is about three times higher than in orientations A and B. The loss from $\mu_{C,eff}$ might originate from the large eddy current generated in the silver inclusion. It is also observed that the complex part of $\mu_{C,eff}$ is slightly higher at

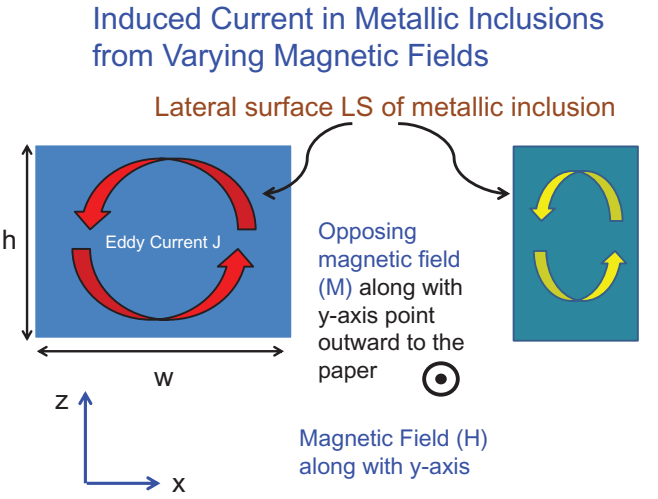

Fig. 10. Two orientations of the metallic inclusions in y–z plane, and the applied magnetic field **H** points inward into the paper. The left figure shows that the orientation provides a larger lateral surfaces LS than the right one. With changing magnetic field **H**, the eddy current **J** is induced, which is proportional to the lateral surfaces LS. The **J** (from opposing magnetic field **M**) is in left diagram is larger than the right one, therefore, the μ_{eff} in left one will be smaller than in the right one.

1 GHz than at 10 GHz. It is possibly related to the higher complex impedance at lower frequency. Therefore, the orientation A is the optimal choice both to obtain high permittivity and permeability. The loss tangents ($\tan(\delta)$) of both ϵ_{eff} and μ_{eff} in this orientation, are very small, in the frequency range of 1–50 GHz.

4. Conclusions

In summary, the shape, orientation and frequency, of the metallic inclusions in a dielectric host, have been theoretically investigated. The square layer (cuboid) with a thin thickness w has been chosen in this study. The three orientations A, B and C were compared. It is found that the orientation A offers the highest relative permittivity and permeability combination, which also give higher values than in cubic inclusions, with the same volume fraction (0.162). Orientation A is the direction of which the propagation arrow (x-axis) is perpendicular to the planar square surface (y–z plane) of the inclusion. The relative $\epsilon_{\text{A,eff}}$ of a substrate has been increased significantly in orientation A (up to $6.254 + 0.0002i$) since the polarization (average electric dipole moment) is the highest. The relative $\mu_{\text{A,eff}}$ can also reach $0.822 + 0.0029i$ because the orientation A reduces the lateral surface area for generating eddy current. Besides, it is found that on the frequency range 1–50 GHz, the loss tangents are small in ϵ_{eff} and μ_{eff}. In future work, we will look for a even smaller inclusions which include quantum mechanical effects in the systems.[42,43]

Acknowledgment

The project was funded by the EPSRC Grant (EP/101490X/1) on synthetic materials and metamaterials studies.

References

[1]J. C. Vardaxoglou, *Frequency Selective Surface: Analysis and Design* (Research Studies Press, Taunton, England, 1997).
[2]W. G. Whittow, S. S. Bukhari, L. A. Jones and I. L. Morrow, Applications and future prospects for microstrip antennas using heterogeneous and complex 3-D geometry substrates, *Prog. Electromagn. Res.* **144**, 271 (2014).
[3]J. C. Vardaxoglou, C. C. Njoku and W. G. Whittow, EM properties of synthetic media, *European Antennas and Propagation Conf.* Gothenburg, Sweden, 710 (2013).
[4]C. C. Njoku, W. G. Whittow and J. C. Vardaxoglou, Effective permittivity of heterogeneous substrates with cubes in a 3-D lattice, *IEEE Antennas Wireless Propag. Lett.* **10**, 1480 (2011).
[5]C. C. Njoku, W. G. Whittow and J. C. Vardaxoglou, Simulation methodology for synthesis of antenna substrates with microscale inclusions, *IEEE Trans. Antennas Propag.* **60**, 2194 (2012).
[6]D. K. Chodgaonkar, V. V. Varadan and V. K. Varadan, Free space measurement of complex permittivity and complex permeability of magnetic materials at microwave frequencies, *IEEE Trans. Instrum. Meas.* **39**, 387 (1990).
[7]E. Tuncer, Dielectric properties of a two dimensional binary system with ellipse inclusion (2002), Availble at http://arxiv.org/pdf/cond-mat/0107618.pdf.
[8]I. Awai, Y. Maegawa and T. Ishizaki, Measurement of effective material constants of artificial dielectrics made of spherical metal particles, *Microwave Conf. (APMC) IEEE* (2009), pp. 1655–1658.
[9]G. Yuan, L. Han, Z. Yu, Y. Liu and P. Lu, Two-dimensional square lattice elliptical dielectric rods photonic crystal bandgap characteristics, *Optical Communications and Networks (ICOCN 2010), 9th Int. Conf.*, China (2010), pp. 399–401.
[10]L. Lewin, The electrical constants of a material loaded with spherical particles, *J. Inst. Elect. Eng.* **94**, 65 (1947).
[11]B. Sareni, L. Krahenbuhl, A. Beroual and C. Brosseau, Effective dielectric constant of random composite materials, *J. Appl. Phys.* **81**, 2375 (1997).
[12]A. H. Sihvola and J. A. Kong, Effective permittivity of dielectric mixtures, *IEEE Trans. Geosci. Remote Sens.* **26**, 420 (1988).
[13]M. Scheller, S. Wietzke, C. Jansen and M. Koch, Modeling heterogeneous dielectric mixtures in the terahertz regime: A quasi-static effective medium theory, *J. Phys. D: Appl. Phys.* **42**, 065415 (2009).
[14]K. Karkkainen, A. Sihvola and K. Nikoskinen, Analysis of a three-dimensional dielectric mixture with finite difference method, *IEEE Trans. Geosci. Remote Sensing* **39**, 1013 (2001).
[15]M. Y. Koledintseva, J. Wu, J. Zhang, J. L. Drewniak and K. N. Rozanov, Representation of permittivity for multiphase dielectric mixtures in FDTD modeling, *EMC 2004 Int. Symp.*, Vol. 1 (2004), pp. 309–314.
[16]Y. I. Li, J. Li, M. J. Wang and Q. F. Dong, The property of Rayleigh scattering for an anisotropic dielectric ellipsoid, *Nat. Sci.* **3**, 48 (2011).
[17]R. C. Jones, A generalization of the dielectric ellipsoid problem, *Phys. Rev.* **68**, 93 (1945).
[18]M. I. Alonso, M. Garriga, F. Alsina and S. Pinol, Determination of the dielectric tensor in anisotropic materials, *Appl. Phys. Lett.* **67**, 596 (1995).
[19]G. E. Jellison Jr. *et al.*, Spectroscopic dielectric tensor of monoclinic crystals: CdWO4, *Phys. Rev. B* **84**, 195439 (2011).
[20]W. R. Tinga, W. A. G. Voss and D. F. Blossey, Generalized approach to multiphase dielectric mixture theory, *J. Appl. Phys.* **44**, 3897 (1973).
[21]D. J. Bergman and Y. Imry, Critical behavior of the complex dielectric constant near the percolation threshold of a heterogeneous material, *Phys. Rev. Lett.* **39**, 1222 (1977).
[22]E. Tuncer, Y. V. Serdyuk and S. M. Gubanski, Dielectric mixtures: Electrical properties and modeling, *IEEE Trans. Dielectr. Electr. Insul.* **9**, 809 (2002).
[23]I. Awai, Artifcial dielectric resonators for miniaturized filters, *IEEE Microw. Mag.* **9**, 55 (2008).
[24]I. Awai *et al.*, An artificial dielectric materials of huge permittivity with novel anisotropy and its application to a microwave BPF, *2003 IEEE MTT-S Int. Microwave Symp. Digest*, Vol. 2 (2003), pp. 1085–1088.
[25]J. D. Jackson, *Classical Electrodynamics*, 3rd edn. (John Wiley and Sons, 1998).
[26]J. M. Geffrin *et al.*, Magnetic and electric coherence in forward- and back-scattered electromagnetic waves by a single dielectric

sub-wavelength sphere, *Nature Commun.* (2012), doi:10.1038/ncomms2167.
[27]J. A. Edminister, *Electromagnetis*, Schaum's Outline Series (McGraw-Hill, 1995).
[28]C. Min *et al.*, Focused plasmonic trapping of metallic particles, *Nature Commun.* **4**, 2891 (2013), doi: 10.1038/ncomms3891.
[29]F. V. Kusmartsev and S. V. Meshkov, Theory of edge optical absorption in crystals, *Sov. Phys. JETP* **67**, 2098 (1989).
[30]R. Turton, *The Physics of Solids* (Oxford University Press, 2000).
[31]E. M. Kiley, V. V. Yakovlev, K. Ishizaki and S. Vaucher, Applicability study of classical and contemporary models for effective complex permittivity of metal powders, *J. Microw. Power Electromagn. Energy* **46**, 26 (2011).
[32]T. Sluka, A. K. Tagantsev, D. Damjanovic, M. Gureev and N. Setter, Enhances electromechanical response of ferroelectrics due to charged domain walls, *Nature commun.* **3**, 748 (2012).
[33]R. Xu, J. Karthik, A. R. Damodaran and L. W. Martin, Stationary domain wall contribution to enhanced ferroelectric susceptibility, *Nature Commun.* **5**, 3120 (2014).
[34]F. V. Kusmartsev, Orbital paramagnetism in two dimensional lattices, *Mod. Phys. Lett. B* **5**, 571 (1991).
[35]D. M. Forrester, K. E. Kuten and F. V. Kusmartsev, Fundamental design paradigms for systems of three interacting magnetic nanodiscs, *Appl. Phys. Lett.* **98**, 163113 (2011).
[36]K. Vynck, D. Felbacq, E. Centeno, A. I. Cbuz, D. Cassagne and B. Guizal, All dielectric rod type meta-materials at optical frequencies, *Phys. Rev. Lett.* **102**, 33901 (2009).
[37]Z. Ku and S. R. Brueck, Comparison of negative refractive index materials with circular, elliptical and rectangular holes, *Opt. Exp.* **15**, 4515 (2007).
[38]A. Alu, A. Salandrino and N. Engheta, Negative effective permeability and left-handed materials at optical frequencies, *Opt. Exp.* **14**, 1557 (2006).
[39]N. G. Alexopoulos, C. A. Kyriazidou and H. F. Contopanagos, Effective parameters for metamorphic materials and metamaterials through a resonant inverse scattering approach, *IEEE Trans. Microw. Theory Tech.* **55**, 254 (2007).
[40]H. Zhou, Y. Li, S. Wang and Y. Wang, An improved method of determining permittivity and permeability by *S* parameters, *PIERS Proc. China* (2009), pp. 768–773.
[41]E. Ekmekci and G. T. Sayan, Investigation of effective permittivity and permeability for a novel V-shaped metamaterial using simulated *S*-parameters, *5th Int. Conf. Electrical and Electronics Engineering*, December 2007; http://www.emo.org.tr/ekler/68fcab5a34b87b6_ek.pdf.
[42]A. M. Zagoskin, A. L. Rakhmanov, S. Savelev and F. Nori, Quantum metamaterials: Electromagnetic waves in josephson qubit lines, *Phys. Status Solid B* **246**, 955 (2009).
[43]A. M. Zagoskin, *Quantum Engineering: Theory and Design of Quantum Coherent Structure* (Cambridge University Press, Cambridge, 2011).